SUPPLEMENTARY FIGURES

SUPPLEMENTARY FIGURE 1

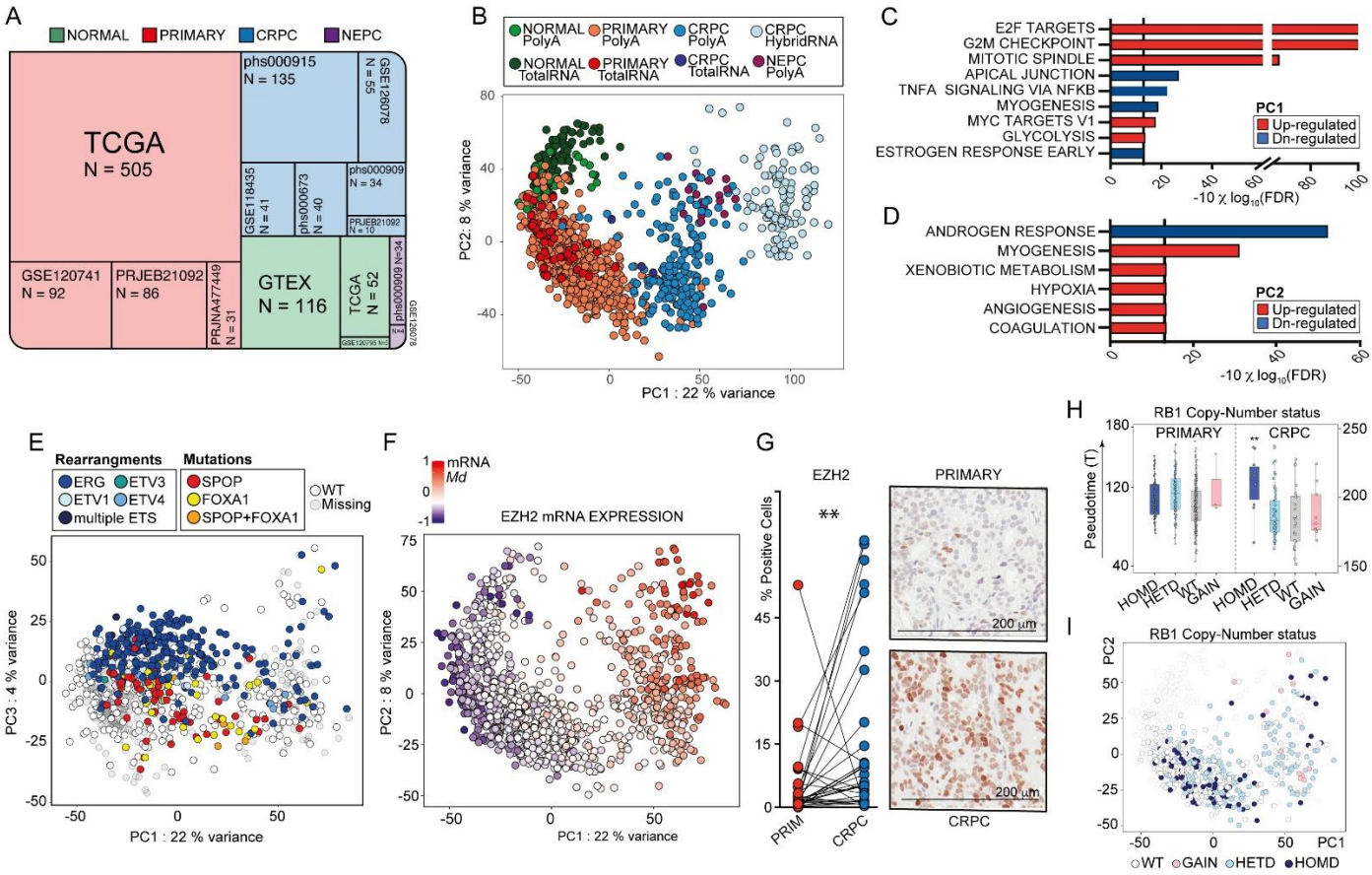

Supplementary Figure 1.

(A) Graphical representation of the RNA sequencing cohorts, their accession numbers, the total number of samples in each dataset, and tumor stages as indicated. **(B)** Position of individual tumors in the PCA after re-processing of the raw data by selecting the top 2000 most variable genes. Hybrid capture-based RNA sequencing samples derived from CPRC highlighted in light blue show a marked but consistent shift in the PC1 and PC2. No significant differences are observed in the first two principal components for TotalRNA when compared to PolyA+ samples. **(C)** Gene-sets enrichments performed using *Camera* algorithm on genes ranked according to their relative contribution (coefficient) to the positioning of samples along the PC1 axis. The analysis performed on Hallmark gene sets reveals an increase of cell cycle-related gene sets along PC1. **(D)** Corresponding analysis performed on genes ranked according to their contribution to PC2 shows a decrease in androgen-responsive genes along this axis. **(E)** PCA plot representing the PC1/PC3 pane can be used to discern SPOP/FOXA1 mutant prostate cancers from those harboring gene fusions involving ETS transcription factors. **(F)** EZH2 mRNA expression increases gradually along the main trajectory. Expression levels of each sample are reported within the PCA plot representing the PC1/PC2 pane. Gene expression levels are scaled between -1 and 1 and are represented in a three-color scale (blue: lowest value; white: median value; red: highest value). **(G)** IHC analysis reveals upregulation of EZH2 in CRPC tumors compared to the matched primary tumors. Left: Quantification of EZH2 positive cells, Right: IHC images of a primary and its corresponding CRPC counterpart. **(H)** Boxplots representing different pseudo-time distribution for RB1-specific copy number alterations (homozygous, heterozygous, wild-type, gains). **(I)** Corresponding PCA plot highlighting RB1 copy-number status across samples.

SUPPLEMENTARY FIGURE 2

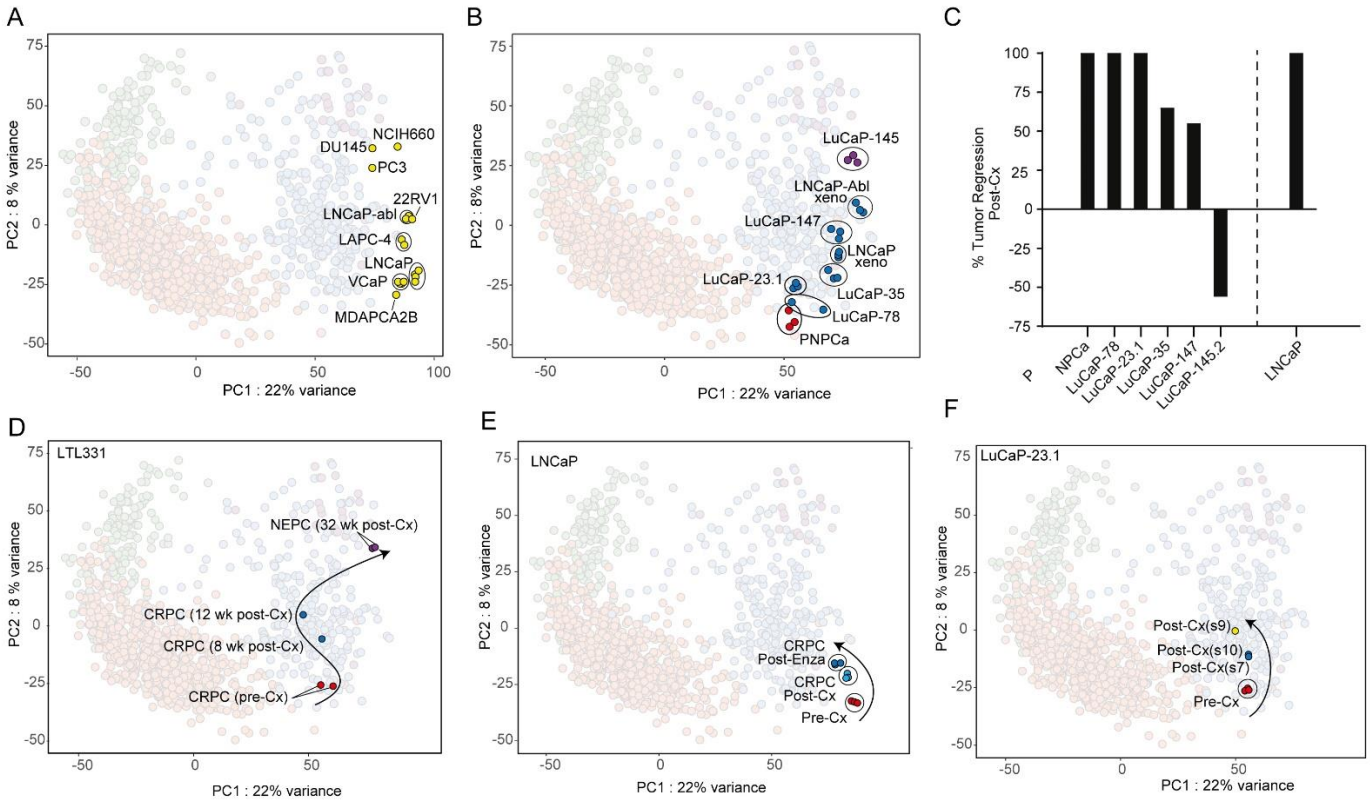

Supplementary Figure 2.

(A) Integration of the indicated ex-vivo cultured prostate cancer cell lines within the PCA plot. (B) Corresponding analysis for Xenografts. For the PNPCa model, the normal and primary tumor tissue's PCA position is reported and dramatically differs from the one found in immune-compromised mice. (C-E) After castration, the indicated PDX models and LNCaP xenograft progress along the main trajectory. Over a time frame of 32 weeks, the LTL331 model reaches terminal neuroendocrine transdifferentiation. See also Figure 4.

SUPPLEMENTARY FIGURE 3

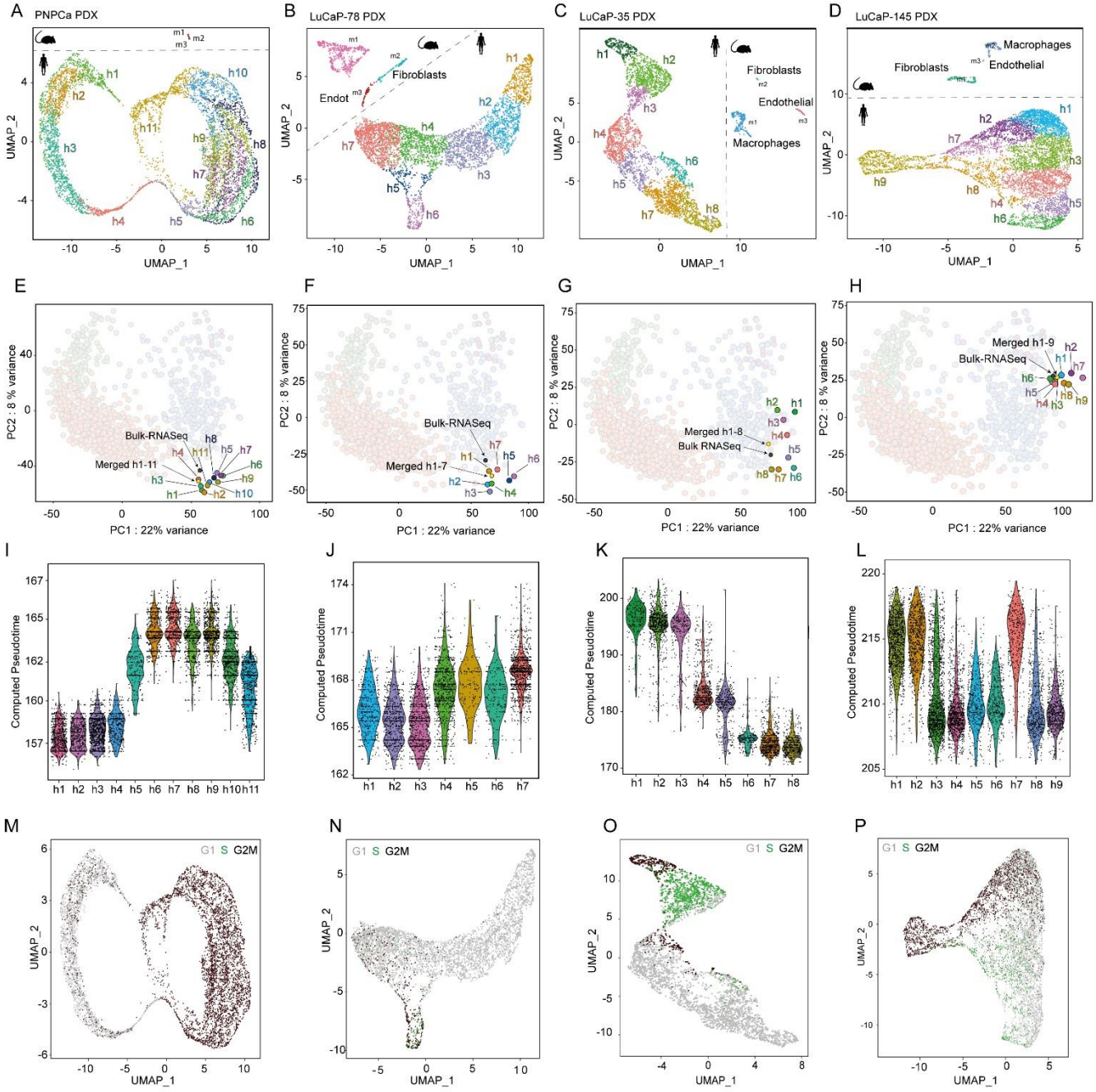

Supplementary Figure 3.

(A-D) Single-cell representation of the indicated PDX models *in vivo* using dimensionality reduction by Uniform Manifold Approximation and Projection (UMAP) and subsequent identification of tumor single-cell clusters using Seurat's workflow. (E-H) The Integration of merged single-cell data of the indicated PDX model on the PCA plot shows a comparable position to the corresponding bulk RNA sequencing data. Individual single-cell clusters are also integrated into the PC1/PC2 pane. The highest dispersion of clusters along the main trajectory is seen for LuCaP-35. (I-L) Violin plots indicating the pseudo-time of individual cells within the different cell clusters. The pseudo-time inference was performed following the imputation of missing genes (dropout events) by using *RMagic*. (M-P) Attribution of cells to either the G1, S, or G2M cell cycle phase for each PDX model. Cell Cycle Phase was determined using Seurat's workflow. Also see Figure 3.

SUPPLEMENTARY FIGURE 4

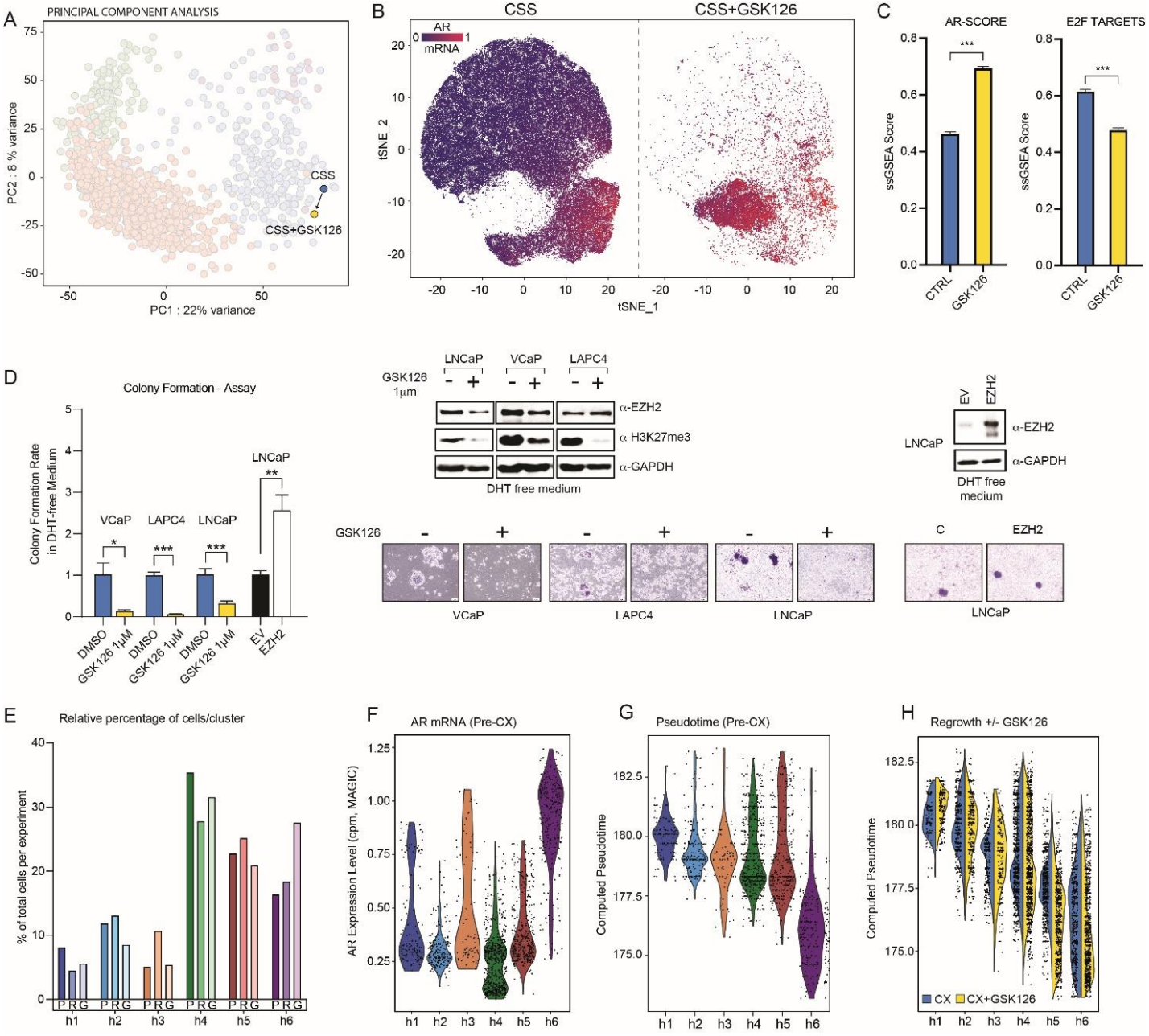

Supplementary Figure 4.

(A) Single-cell RNASeq data of LNCaP cells cultured in charcoal-stripped serum (CSS) was merged and integrated within the PCA plot (PC1/PC2). PCA positioning shows a decrease in pseudo-time upon EZH2 inhibition by GSK126. (B) Dimensionality reduction (TSNE) of single-cell RNASeq performed on LNCaP cells cultured in vitro with charcoal-stripped serum (CSS) in the presence (right) or absence (left) of the EZH2 inhibitor GSK126. Upon GSK126 treatment, as most cell clusters disappear, there is an increase in AR mRNA expression in the transcriptionally rewired LNCaP cells that give rise to a novel cluster characterized by higher AR expression levels. (C) Corresponding quantification of AR-SCORE and E2F target genes (Hallmark gene set) computed for each cell before (left) and following (right) EZH2 inhibition by GSK126. Missing gene-expression values (dropout events) for each cell were imputed using *RMagic*. (D) GSK126 inhibits colony formation of LNCaP cells when cultured in CSS, while EZH2 over-expression increases the number of colonies under the same condition. (E) Following EZH2 inhibition by GSK126, there is a common trend towards decreasing of cells in most clusters, except for cluster h6, which shows an opposite behavior. (F) Violin plots depicting AR expression levels show that the h6 cell cluster is characterized by higher levels of the latter. Missing gene-expression values (dropout events) for each cell were imputed using *RMagic*. (G) The pseudo-time inference was performed for each cell, and cluster h6 resulted to be associated with a less progressed phenotype. (H) Violin plots comparing pseudo-time before (blue) or following (yellow) EZH2 inhibition by GSK126. Cluster h6 displays the highest AR expression levels, the least progression on the main trajectory, and a reduction in pseudo-time after GSK126 treatment. Significance was assessed using the Wilcoxon sum-rank test and p-values were adjusted for multiple comparisons using false discovery rate (FDR): * < 0.05, ** < 0.01, *** < 0.001. Also see Figure 6.